

G51169 Electronic Supplement ES1

Analytical methods
Sample descriptions
Mineral trace elements and thermobarometry
Table S1
Table S2
Figure S1

Analytical methods

Fluid-mobile elements (FME: Li, B, F, Cl) concentrations and B isotope ratios of olivine were measured in-situ in thick (~ 50 µm) sections by Secondary Ion Mass Spectrometry (SIMS) at the Edinburgh Ion Microprobe Facility using a Cameca IMS-4f and a Cameca IMS-1270, respectively, following the methods detailed in Supplementary Information of Clarke et al. (2020). Boron isotope measurements of olivine and serpentine were calibrated using matrix-matched standards.

A small LA-ICP-MS dataset of olivine, serpentine and chromite in the same samples was obtained using a Thermo Element II with a New Wave Excimer prototype laser system at Oxford University following the methods in De Hoog et al. (2010), which provided additional trace elements.

Electron microprobe data for the samples was presented by Hattori et al. (2010) and was supplemented by a small number of analyses using a Cameca SX100 at the University of Edinburgh, see Clarke et al. (2020) for analytical details.

Sample descriptions (petrography and B contents)

Table S1. Brief sample descriptions

Sample	Rock type	Assemblage ^a	Texture	Late-stage overprint
HC123	Dunite	Ol 94, Cr 6, Chl <1	Fine grained, disseminated chromite	Pervasive, extensive veining (ca. 20%)
HC87	Atg dunite	Ol 96, Atg 2, Cr 1.5	Porphyroclastic	Pervasive, extensive veining (ca 45%)
HSS46	Atg dunite	Ol 83, Atg 16, Cr 1	Porphyroclastic	Extensive veining, mesh (ca. 40%)
HSS73	Atg dunite	Ol 79, Atg 20, Cr 1	Fine grained, foliated	Nearly absent, no veining
HC104	Atg serpentinite	Ol 48, Atg 51, Cr 1	Porphyroclastic, foliated	Limited to grain boundaries (ca. 10%)

^a Mineral assemblage prior to late-stage overprint, numbers indicate modal percentages. Atg = antigorite, Cr = chromite, Ol = olivine, Chl = chlorite

HC123: Fine-grained (some larger grains highly fractured) olivine with no antigorite but rare chlorite flakes, slightly oriented, abundant chromite in large fine-grained seams and patches, pervasive late-stage veining of lizardite (several mm in width) cross-cutting the matrix. Olivine: Low B (avg 2 µg/g), $\delta^{11}\text{B}$ ca. -4 excl 1 outlier of -10. Small concentration range (1-5 µg/g). The sample also contains

chlorite as small grains in the matrix, but no antigorite. Extensive late-stage veining with high B (32-117 µg/g).

HC87: Fairly coarse-grained with sparse small blades of antigorite (<2 modal%) and no apparent foliation. Not always clear what are fractured remnants of large grains or neoblasts. Very pervasive late-stage veining in multiple generations affecting much of the samples but large unaltered patches are present. Large porphyroclastic olivine most have large amounts of small needle-like inclusions, probably serpentine. Olivine has large variation in B contents with large (> 150 µm) grains having fairly uniform low B (0.5-1 µg/g) with slight increase from core to rim (up to 6 µg/g), but smaller grains have ca. 8-13 µg/g. No correlation with proximity to wide lizardite veins.

HSS46: (near the serpentinite border) Generally fine-grained with some patches of coarse olivine and large (several mm) antigorite blades (ca. 20% overall). Very pervasive late-stage veining and mesh of lizardite. Chromite with magnetite rims. No strong foliation. Olivine is mostly fine-grained but a large 2mm porphyroclasts show core to rim zoning of B (2-16 µg/g). Another porphyroclastic olivine grain, containing lizardite mesh has low B (2 µg/g) even though it's directly adjacent to mesh with 24 µg/g B. Antigorite has 9-38 µg/g B.

HSS73: strong foliation, nearly completely neoblastic olivine (range ca. 100-250 µm) apart from several relict mm-sized porphyroclasts, abundant fine antigorite needles (ca. 10%), very limited late overprint with no veining having developed. Olivine: three core-rim B profiles although only one with isotopes. Cores have low B but vary (two grains 5-7 µg/g, one other only 1.5 µg/g), but rims are similar and also similar to neoblasts (10-15 µg/g). Note that the sample has abundant antigorite needles but no lizardite veining, providing strong evidence that B in olivine is not a late-stage overprint.

HC104: strongly foliated, but abundant large olivine porphyroclasts. Pervasive fine-grained antigorite needles with some coarse-grained (>1 mm) locally, often segregating into veins/bundles (ca. 30% overall). Late-stage veining limited, lizardite mostly fills cracks in olivine and grain boundaries in matrix. Olivine B: 3 core-rim points 200-400 µm apart. Data quite variable for cores and rims, although generally B goes up. The low core concentration (1 µg/g B) is from a lasered grain, but the rim is uncertain, big discrepancy between 4f and 1270 (12 vs 2.5 µg/g). Two other grain have higher cores (5-7 µg/g) but core-rim less clear for one. The other one was previously lasered (two holes, data identical) but little B variation. Neoblasts variable but high and cover range of rims (8-20 µg/g B).

Mineral trace elements and thermobarometry

Olivine

All samples contain primary mantle olivine (Fo90-94). Concentrations of trace elements in olivine of various metals such as Sc (1-3 µg/g), MnO 0.10-0.12 wt.%), NiO (0.35-0.38 wt.%), Zn (10-40 µg/g) and Co (110-140 µg/g) are typical of mantle peridotites although Cu contents (ca. 0.1µg/g) appear low (De Hoog et al., 2010).

Temperature-sensitive elements in olivine, such as Na (<10 µg/g), Al (<4 µg/g), Ca (20-40 µg/g), V <0.5 µg/g) and Cr (4-10 µg/g) are extremely low, equivalent to equilibration at ca. 600 °C (De Hoog et al., 2010), which most likely represents closure temperatures during slow cooling of the body. Titanium contents are typical values of depleted spinel peridotites but vary per sample, with olivine in HC123 (20-70 µg/g) markedly higher Ti than olivine in the other samples (<10 µg/g). Low Y

contents ($<0.01 \mu\text{g/g}$) and Zr ($<0.025 \mu\text{g/g}$) are consistent with the highly residual nature of the dunites. In contrast, Li contents (**Fig. S1**) are typical of mantle olivine, with HC123 and HC104 having somewhat higher Li ($2\text{--}4 \mu\text{g/g}$) than other samples (ca. $1.5 \mu\text{g/g}$). These two samples also have high F contents (HC123: $40\text{--}70 \mu\text{g/g}$; HC104: $6\text{--}30 \mu\text{g/g}$) compared to other samples (mostly $1\text{--}10 \mu\text{g/g}$) (**Fig. 2**). Boron concentrations are variable and significantly above typical mantle olivine value $<0.1 \mu\text{g/g}$ (Kent and Rossman, 2002). The two most B-enriched samples (HC104 and HSS73) are also high in Cl (>6 vs $<5 \mu\text{g/g}$ for other samples) (**Fig. S1**).

Antigorite occurring as small lath-shaped crystals in the sample matrix have high Mg# (0.95-0.97), high Al_2O_3 (0.2-1.1 wt%) and variably Cr (0.03-0.44 wt%), which indicates that the partial breakdown of chromite may be involved in its formation. Lithium contents are very low ($<0.2 \mu\text{g/g}$), which is common in subduction-related serpentinites (e.g., Clarke et al., 2020). It has low Cl contents (generally $<30 \mu\text{g/g}$) and generally low F ($<100 \mu\text{g/g}$) except in sample HC104 which has ca. $250 \mu\text{g/g}$ F. Antigorite also has notably high As ($0.7\text{--}2 \mu\text{g/g}$) and Sb ($0.2\text{--}0.3 \mu\text{g/g}$).

Chlorite was only observed in antigorite-free sample HC123, where it occurs as rare small flakes in the matrix. It is characterised by high Ti ($100\text{--}150 \mu\text{g/g}$), high F ($400\text{--}600 \mu\text{g/g}$) but low Cl contents ($30\text{--}100 \mu\text{g/g}$). Boron contents are similar to olivine from the same sample ($1\text{--}5 \mu\text{g/g}$).

In comparison to antigorite, lizardite has low Al (0.002-0.10 wt.%) and Cr (<0.001 wt.), and low As and Sb but somewhat higher Li. Apart from HC123, samples have elevated Li ($0.5\text{--}2 \mu\text{g/g}$) in lzd veins compared to atg. Lizardite veins have elevated Cl ($60\text{--}900 \mu\text{g/g}$) compared to atg, but are highly variable, up to an order of magnitude in most samples. Some lzd veins (HC123, HC104) also have high F but its variable and does not correlate with Cl.

Chromite compositions are similar in all samples, with high Cr# (0.7-0.8) and low Mg# (0.3-0.5). Sample HC123 has somewhat high TiO_2 (0.4 wt.%) compared to other samples (0.04-0.14 wt%) with somewhat lower V and Sc contents.

Spinel-olivine thermometry of Ballhaus et al. (1991) for sample HC123 yields 670°C (Ballhaus et al., 1991) This is a typical value for spinel-olivine pairs from slowly exhumed terranes (e.g., Chen et al., 2020; De Hoog et al., 2009) and represents the temperature when Fe-Mg exchange between olivine and spinel becomes so slow that it no further re-equilibrates during cooling of the rock (i.e., a closure temperature rather than equilibration temperature). The oxygen fugacity is high ($\Delta\text{NNO} + 1.5$).

Table S2. Calculated bulk rock FME contents (excluding secondary overprint)

sample	Li ($\mu\text{g/g}$)	1s	B ($\mu\text{g/g}$)	1s	F ($\mu\text{g/g}$)	1s	Cl ($\mu\text{g/g}$)	1s
HC123	2.4	± 0.2	2.1	± 0.3	52	± 3	3.3	± 0.4
HC87	1.4	± 0.1	3.9	± 1.1	8.2	± 1.2	4.8	± 1.5
HSS46	1.3	± 0.1	4.9	± 0.6	15	± 2	4.8	± 1.2
HSS73	1.4	± 0.3	9.4	± 1.9	13	± 2	9.9	± 3.8
HC104	1.8	± 0.2	9.1	± 1.1	138	± 2	9.4	± 2.0

1s uncertainties based on propagated uncertainties of multiple analyses of mineral grains and mineral modes.

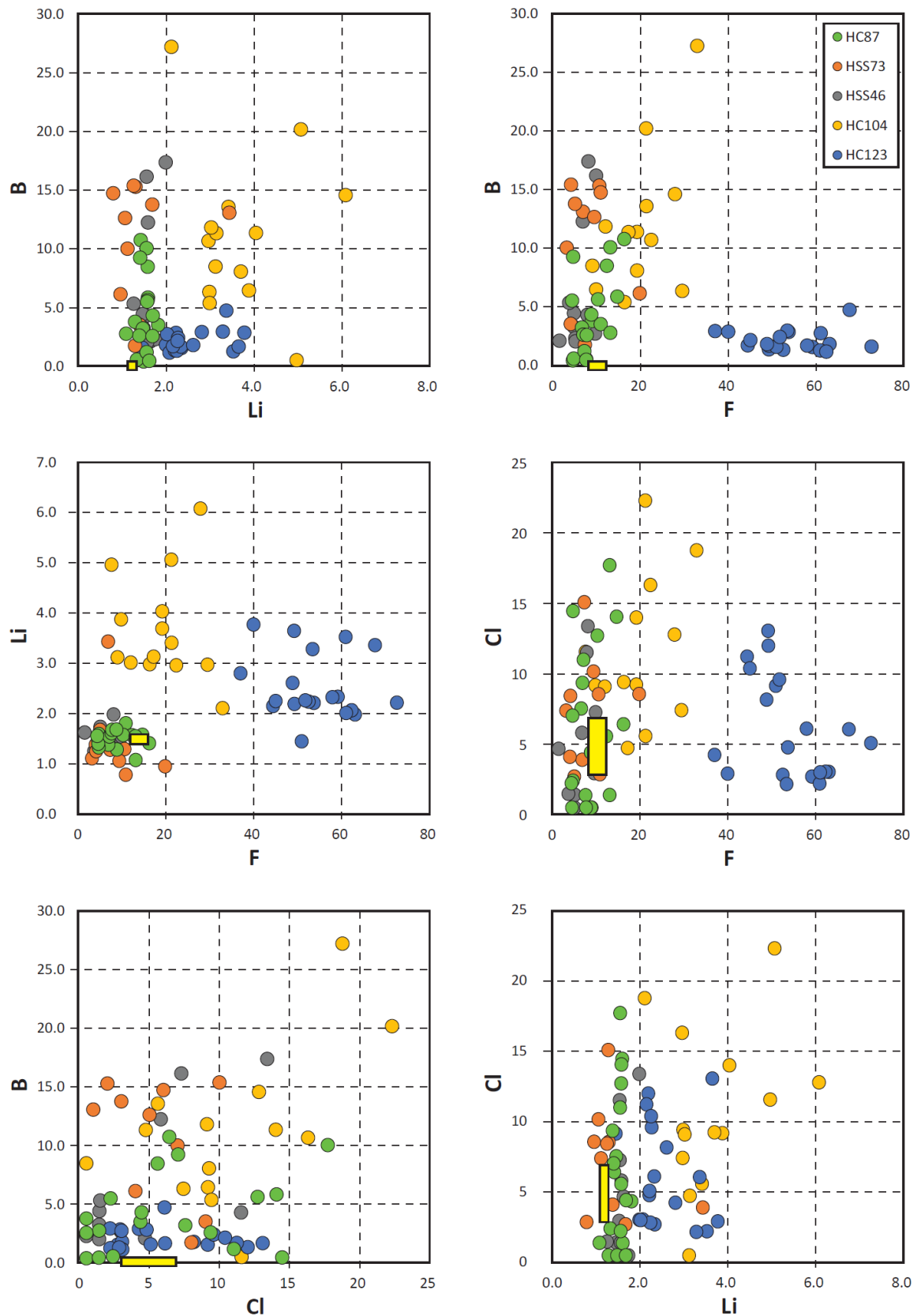


Fig. S1 Fluid-mobile element (Li, B, F, Cl) systematics of olivine in Higashi-akaishi metaperidotites. The composition of average depleted mantle $\pm 1s$ is indicated by a yellow rectangle (Kendrick et al., 2017; Marschall et al., 2017).

References

- Ballhaus, C., Berry, R. F., and Green, D. H., 1991, High-pressure experimental calibration of the olivine-ortho-pyroxene-spinel oxygen geobarometer - Implications for the oxidation-state of the upper mantle: *Contributions to Mineralogy and Petrology*, v. 107, no. 1, p. 27-40,
- Chen, C., De Hoog, J. C. M., Su, B.-X., Wang, J., Uysal, İ., and Xiao, Y., 2020, Formation process of dunites and chromitites in Orhaneli and Harmancik ophiolites (NW Turkey): Evidence from in-situ Li isotopes and trace elements in olivine: *Lithos*, v. 376-377, p. 105773, 10.1016/j.lithos.2020.105773
- Clarke, E., De Hoog, J. C. M., Kirstein, L. A., Harvey, J., and Debret, B., 2020, Metamorphic olivine records external fluid infiltration during serpentinite dehydration: *Geochemical Perspectives Letters*, v. 16, p. 25-29, 10.7185/geochemlet.2039
- De Hoog, J. C. M., Gall, L., and Cornell, D. H., 2010, Trace-element geochemistry of mantle olivine and application to mantle petrogenesis and geothermobarometry: *Chemical Geology*, v. 270, no. 1-4, p. 196-215, DOI 10.1016/j.chemgeo.2009.11.017
- De Hoog, J. C. M., Janak, M., Vrabec, M., and Froitzheim, N., 2009, Serpentinised peridotites from an ultrahigh-pressure terrane in the Pohorje Mts. (Eastern Alps, Slovenia): Geochemical constraints on petrogenesis and tectonic setting: *Lithos*, v. 109, no. 3-4, p. 209-222,
- Hattori, K., Wallis, S., Enami, M., and Mizukami, T., 2010, Subduction of mantle wedge peridotites: Evidence from the Higashi-akaishi ultramafic body in the Sanbagawa metamorphic belt: *Island Arc*, v. 19, no. 1, p. 192-207, 10.1111/j.1440-1738.2009.00696.x
- Kendrick, M. A., Hemond, C., Kamenetsky, V. S., Danyushevsky, L., Devey, C. W., Rodemann, T., Jackson, M. G., and Perfit, M. R., 2017, Seawater cycled throughout Earth's mantle in partially serpentinized lithosphere: *Nature Geosci*, v. 10, no. 3, p. 222-228, 10.1038/ngeo2902
- Kent, A. J. R., and Rossman, G. R., 2002, Hydrogen, lithium, and boron in mantle-derived olivine: The role of coupled substitutions: *American Mineralogist*, v. 87, no. 10, p. 1432-1436,
- Marschall, H. R., Wanless, V. D., Shimizu, N., von Strandmann, P. A. E. P., Elliott, T., and Monteleone, B. D., 2017, The boron and lithium isotopic composition of mid-ocean ridge basalts and the mantle: *Geochimica Et Cosmochimica Acta*, v. 207, p. 102-138, 10.1016/j.gca.2017.03.028